

# Spinocerebellar Ataxia Type 6 Protein Aggregates Cause Deficits in Motor Learning and Cerebellar Plasticity

Melanie D. Mark,<sup>1\*</sup> Martin Krause,<sup>1\*</sup> Henk-Jan Boele,<sup>2</sup> Wolfgang Kruse,<sup>1</sup> Stefan Pollok,<sup>1</sup> Thomas Kuner,<sup>3</sup> Deniz Dalkara,<sup>4</sup> Sebastiaan Koekkoek,<sup>2</sup> Chris I. De Zeeuw,<sup>2,5</sup> and Stefan Herlitze<sup>1</sup>

<sup>1</sup>Department of Zoology and Neurobiology, Ruhr University Bochum, D-44780 Bochum, Germany, <sup>2</sup>Department of Neuroscience, Erasmus Medical Center, 3000 DR Rotterdam, The Netherlands, <sup>3</sup>Department of Functional Neuroanatomy, Institute of Anatomy and Cell Biology, Heidelberg University, D-69120 Heidelberg, Germany, <sup>4</sup>Vision Institute, F-75012 Paris, France, and <sup>5</sup>Netherlands Institute for Neuroscience, Royal Dutch Academy of Arts and Sciences, 1105 BA Amsterdam, The Netherlands

Spinocerebellar ataxia type 6 (SCA6) is linked to poly-glutamine (polyQ) within the C terminus (CT) of the pore-forming subunits of P/Q-type Ca<sup>2+</sup> channels (Ca<sub>v</sub>2.1) and is characterized by CT protein aggregates found in cerebellar Purkinje cells (PCs). One hypothesis regarding SCA6 disease is that a CT fragment of the Ca<sub>v</sub>2.1 channel, which is detected specifically in cytosolic and nuclear fractions in SCA6 patients, is associated with the SCA6 pathogenesis. To test this hypothesis, we expressed P/Q-type channel protein fragments from two different human CT splice variants, as predicted from SCA6 patients, in PCs of mice using viral and transgenic approaches. These splice variants represent a short (CT-short without polyQs) and a long (CT-long with 27 polyQs) CT fragment. Our results show that the different splice variants of the CTs differentially distribute within PCs, i.e., the short CTs reveal predominantly nuclear inclusions, whereas the long CTs prominently reveal both nuclear and cytoplasmic aggregates. Postnatal expression of CTs in PCs in mice reveals that only CT-long causes SCA6-like symptoms, i.e., deficits in eyeblink conditioning (EBC), ataxia, and PC degeneration. The physiological phenotypes associated specifically with the long CT fragment can be explained by an impairment of LTD and LTP at the parallel fiber-to-PC synapse and alteration in spontaneous PC activity. Thus, our results suggest that the polyQ carrying the CT fragment of the P/Q-type channel is sufficient to cause SCA6 pathogenesis in mice and identifies EBC as a new diagnostic strategy to evaluate Ca<sup>2+</sup> channel-mediated human diseases.

**Key words:** P/Q type calcium channel; poly-glutamine disease; spinocerebellar ataxia type 6

## Introduction

In both human and mouse, numerous missense mutations in the P/Q-type Ca<sup>2+</sup> channel sequence have been identified and linked to neurological defects (Pietrobon, 2005). In humans, mutations of the P/Q-type Ca<sup>2+</sup> channel sequence lead to dominantly inherited neurological diseases that manifest as migraines in familial hemiplegic migraine-1, episodic ataxia, and epilepsy in episodic ataxia type 2, and to pure cerebellar ataxia in spinocerebellar ataxia type 6 (SCA6; Bidaud et al., 2006; Pietrobon, 2010). SCA6 has been identified as a poly-glutamine (polyQ) disease in which 21–33 residues are found in exon 47 of the P/Q-type chan-

nel C terminus (CT; Zhuchenko et al., 1997; Zoghbi and Orr, 2000; Mantuano et al., 2003). In humans, exon 47 undergoes alternative splicing, leading to C-terminal isoforms containing either exon 47 alone or with the polyQ repeats (Zhuchenko et al., 1997). Protein aggregates containing the CT are present in the nucleus, cell bodies, and dendrites of Purkinje cells (PCs) SCA6 patients (Ishikawa et al., 1999a, 2001; Ishiguro et al., 2010).

Two main disease-related hypotheses have been suggested for CT-containing protein fragments found in SCA6 patients. First, the CT-containing proteins may constitute a degradation product of the channel that is more stable and therefore enriched in the disease form (Bidaud et al., 2006). This hypothesis is supported by the fact that CT domains of the Ca<sub>v</sub>α<sub>1</sub>2.1 subunit are susceptible to proteolytic processing (Kubodera et al., 2003; Kordasiewicz et al., 2006). Indeed, when Ca<sub>v</sub>α<sub>1</sub>2.1 subunits are expressed in HEK293 cells, the presence of 60–75 kDa peptides can be recognized by an antibody to the CT domain (Kubodera et al., 2003), and subunits carrying polyQ residues with different lengths (11 and 27) show differences in the stability of the proteolytic products (Kubodera et al., 2003). Second, the CACNA1A gene encoding the α<sub>1A</sub> subunit may contain a transcription factor with an altered function in the disease form (Du et al., 2013). This hypothesis has been derived from the observation that the CT-containing the polyQ stretch can induce a form of cell death that depends on its nuclear localization (Kordasiewicz et al.,

Received March 7, 2015; revised April 27, 2015; accepted May 2, 2015.

Author contributions: M.D.M., M.K., H.-J.B., S.K., C.I.D.Z., and S.H. designed research; M.D.M., M.K., W.K., and S.P. performed research; H.-J.B., T.K., D.D., and S.K. contributed unpublished reagents/analytic tools; M.D.M., M.K., W.K., S.P., and S.H. analyzed data; M.D.M., C.I.D.Z., and S.H. wrote the paper.

This work was supported by German Research Foundation Grants He2471/8-1 (S.H.) and Ma5806/1-1 (M.D.M.), SFB 874 project B10 (S.H.), the Dutch Organization for Medical Sciences (The Netherlands Organization for Health Research and Development) and Life Sciences, Senter (Neuro-Basic), and European Resuscitation Council Advanced of the European Community (C.I.D.Z.). We thank Stefan Dobers, Stephanie Krämer, Margareta Möllmann, Volker Rostek, and Manuela Schmidt for excellent technical assistance.

\*M.D.M. and M.K. contributed equally to this work.

The authors declare no competing financial interests.

Correspondence should be addressed to Dr. Melanie D. Mark, Department of Zoology and Neurobiology, ND7/31, Ruhr University Bochum, Universitätsstrasse 150, D-44780 Bochum, Germany. E-mail: melanie.mark@rub.de.

DOI:10.1523/JNEUROSCI.0891-15.2015

Copyright © 2015 the authors 0270-6474/15/358882-14\$15.00/0

2006). Interestingly, this CT-containing protein peptide can be generated by a bicistronic mRNA of the Cav2.1  $\alpha$  subunit that functions as a transcription factor to control expression of PC genes but reduces viability of PCs and induces cerebellar atrophy in the disease form (Du et al., 2013).

Cerebellar syndromes in SCA6 patients, such as ataxia of gait and stance, dysmetria, and oculomotor deficits, most likely develop as a result of changes in cerebellar output (De Zeeuw et al., 2011). The deficits in cerebellar function in SCA6 patients are suggestive for impairments in eyeblink conditioning (EBC), a form of associative motor learning that depends on the integrity of cerebellar synaptic plasticity (Kim and Thompson, 1997; Boele et al., 2010).

To analyze the physiological and behavioral consequences of CT polypeptides as predicted and found in SCA6 patients, i.e., CT-short (ending at exon 46) and CT-long polyQ (ending at exon 47 and containing 27 polyQ residues), we exogenously expressed the human CT polypeptides in mouse cerebellar PCs using viral and transgenic approaches. Our findings reveal that, as in SCA6 patients, a clustering of the CTs in nuclear inclusions and cytoplasmic aggregates occurred in infected PCs. Postnatal expression of the disease peptide causes SCA6 symptoms, including ataxia and PC degeneration, that are correlated with altered PC firing *in vivo*. Most importantly, expression of the SCA6 peptide causes a virtually complete loss of EBC that is correlated with the loss of cerebellar plasticity (i.e., LTP and LTD) at the parallel fiber (PF)-to-PC synapse. Thus, our results describe for the first time the physiological consequences of the human polyQ CT peptide as found in SCA6 patients on cerebellar plasticity. In addition, this study identifies an alteration in EBC as a new diagnostic strategy to detect Ca<sup>2+</sup> channel-mediated diseases at an early disease state.

## Materials and Methods

The constructs for the human Ca<sub>v</sub>α<sub>1</sub>2.1 subunit corresponding to short or long isoforms were a generous gift from Dr. Cheng Chi Lee (University of Texas-Houston Medical School, Houston, TX). The Ca<sub>v</sub>α<sub>1</sub>2.1 short ends at exon 46, whereas the long isoforms contain an additional pentanucleotide sequence before the stop codon (GGCAG), inducing a frame shift. Therefore, the long isoforms express the additional exon 47. The full-length Ca<sub>v</sub>α<sub>1</sub>2.1 subunits were cloned from the original vectors into pcDNA3.1<sup>+</sup> via BamHI-XbaI sites and encodes the last 550 aa from the P/Q-type channels. From the Ca<sub>v</sub>α<sub>1</sub>2.1 subunit, full-length sequences from the CTs were excised via BglII-XhoI sites, cloned into phosphorylated enhanced yellow fluorescent protein (YFP)-C2, and the YFP-tagged CT was inserted into phosphorylated adeno-associated virus 2 (pAAV2).

### AAV2 virus production and virus injection

YFP-CT-short and YFP-CT-longQ27 were cloned into pAAV-MCS (Stratagene). AAV2 production was performed as described previously (Spoida et al., 2014). Briefly, low-passage AAV HEK293 cells were cotransfected with equimolar amounts of pAAV-CT-short/CT-longQ27, pAAV-RC, and pHelper using calcium phosphate-based protocol. Three days after transfection, cells were removed from the dishes, pelleted (3000 × g, 10 min, room temperature), resuspended in 7.5 ml of lysis buffer (150 mM NaCl and 50 mM Tris-HCl, pH 8.5), and lysed via three freeze/thaw cycles in dry ice/ethanol and 37°C water bath (each 10 min). To get rid of free DNA, cell suspension was treated with 50 U of benzonase endonuclease (Sigma) for 2 h at 37°C. The cell debris was spun down at 4500 rpm for 15 min at 4°C. The supernatant was collected in a syringe and filtered into a 15 ml falcon tube through a 0.45 μm filter unit to obtain the crude lysate. Recombinant virus particles were purified from crude lysate using heparin-agarose columns according to the procedure of the manufactures (catalog #732-1010; Bio-Rad). The virus solution was concentrated with a centrifugation step (4500 rpm) until <500 μl were left, and aliquots were stored at 4°C until additional use. AAVs expressing YFP-CT-

short and YFP-CT-longQ27 were injected into cerebellar cortex of 3- to 4-week-old male ( $n = 5$ ) C57BL/6 mice. Mice were anesthetized deeply with an intraperitoneal injection of a ketamine (10 mg/kg)/xylazine (20 mg/kg) and placed into a stereotactic frame (Stoelting). The skin was opened with a sagittal incision along the midline. A small craniotomy was performed for implantation using a micro drill. A customized glass pipette attached to a 5 ml syringe was used for virus delivery at −6.5 mm posterior and 0 mm lateral to bregma at a depth of 1.5 mm. At the end of the injection, the skin was sutured. After the surgery, animals received subcutaneous injection of carprofen (2 mg/kg) for analgesia. Animals were placed individually into their home cages and allowed to recover for at least 7 d.

### Microscopy and image analysis

The distribution of the YFP-tagged Ca<sub>v</sub>α<sub>1</sub>2.1 CT proteins in cerebellar slices was analyzed using a Leica TCS SP5 confocal laser scanning microscope (DMI6000 B; Leica) interfaced to a personal computer, running Leica Application Suite Advanced Fluorescence software (LAS AF 2.6). A 10×/0.3 numerical aperture (NA), 20×/0.7 NA, or 40×/1.1 NA objective was used to capture all photomicrographs. Sequential z-stacks were made for each section, and crosstalk of the fluorophores was eliminated automatically with LAS AF software. YFP fluorescence was detected by excitation with an argon laser (laser line 514 nm). Slow-fade with DAPI (Invitrogen) was used as mounting medium to label the nuclei of HEK293 cells and was detected by excitation with a diode laser at 405 nm. HEK293 cells were fixed for 10 min with a 4% formaldehyde solution (Sigma) in PBS, followed by PBS washes. Coverslips were mounted with Slow-Fade DAPI and left at room temperature overnight. For long-term storage, sealed coverslips were kept at 4°C. DAPI and CT YFP fluorescence was also detected on the upright Leica DMSFA using a 63× water objective (1.2 NA) coupled to a DG5 light source (Sutter Instruments). The following Chroma filter sets were used (excitation, dichroic, emission, respectively): DAPI: D350, 50×, 400DCLP, D460/50M; YFP: HQ500/20s, Q151LP, HQ535/30m. Image analysis and deconvolution of images were performed using Velocity software.

### Electrophysiology

For recordings of EPSCs in PCs, whole-cell voltage-clamp recordings were made at 30°C from cerebellar slices as described previously (Womack and Khodakhah, 2003; Mark et al., 2011; Maejima et al., 2013). Parasagittal cerebellar slices (250 μm thick) were prepared on a Leica VT 1000S vibratome from at least four 21- to 32-d-old male mice. PCs were identified visually under an upright microscope (BX51 WI; Olympus) equipped with infrared illumination. During experiments, slices were perfused continuously with an artificial CSF (aCSF) containing the following (in mM): 125 NaCl, 2.5 KCl, 2 CaCl<sub>2</sub>, 1 MgSO<sub>4</sub>, 26 NaHCO<sub>3</sub>, 1.25 NaH<sub>2</sub>PO<sub>4</sub>, and 20 D-glucose (equilibrated with 95% O<sub>2</sub> and 5% CO<sub>2</sub>). Borosilicate glass electrodes (2–4 MΩ) were filled with an internal solution containing the following (in mM): 60 CsCl, 10 D-gluconic acid, 20 tetraethylammonium-Cl, 30 HEPES, 20 BAPTA, 4 MgCl<sub>2</sub>, 4 ATP, and 0.4 GTP, pH 7.3, adjusted with CsOH for EPSC measurements. Picrotoxin (100 μM; Tocris Bioscience) was added to the external solution to block GABA<sub>A</sub> receptor-mediated inhibitory synaptic transmission, and 5 mM QX314 was added to the internal solution to block voltage-gated Na<sup>+</sup> currents in PCs. For EPSC recordings, PCs were voltage clamped at −60 mV and were evoked by 100 μs voltage pulses applied through a glass pipette filled with aCSF and placed in the molecular layer for PF-EPSCs or in the vicinity of PC somata for climbing fiber-EPSCs. For LTD and LTP measurements, EPSCs were elicited every 30 s for at least 5 min before LTD or LTP was induced. For induction of LTD, PCs were voltage clamped at −10 mV and 150 PF stimuli at 0.5 Hz were applied, whereas PCs were voltage clamped at −60 mV and 150 PF stimuli at 1 Hz were applied to induce LTP. After the stimulation protocol, EPSCs were recorded every 30 s for 30 min at −60 mV. CNQX at 20 μM was applied at the end of every experiment to demonstrate that EPSCs mainly consist of AMPA receptor currents. For loose-patch recordings, pipettes were filled with aCSF. Picrotoxin (100 μM; Tocris Bioscience) and CNQX (10 μM; Tocris Bioscience) were added to bath solution to block synaptic currents. Visually identified PCs were measured at seal resistances >150 MΩ

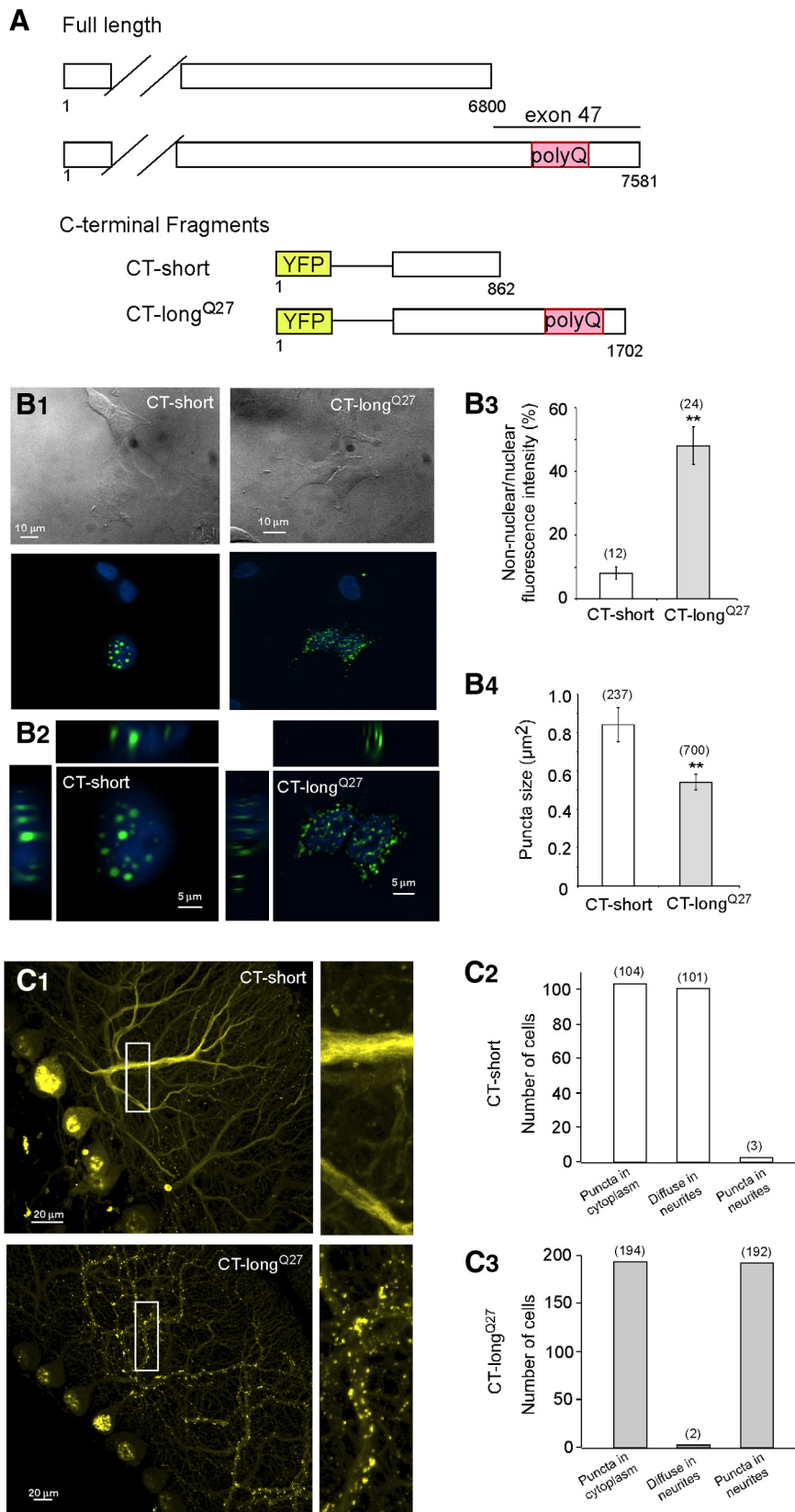


**Figure 1.** CT-short predominantly targets to the nucleus, whereas CT-longQ27 is found in both the cytoplasm and the nucleus in HEK293 cells and cerebellar PCs. **A**, Schematic of the human  $Ca_v2.1$  isoforms and the derived C-terminal constructs as predicted and observed in SCA6 patients. Top, Full-length (FL) cDNAs of the human  $Ca_v2.1$  isoforms reveal the different splice variants. FL-short ends after exon 46, whereas FL-longQ27 contains the coding sequence of the additional exon 47. The polyQ stretch (27 polyQs) is located within exon 47. Bottom, The different CTs were fused to YFP. **B**, CT-short is targeted to the nucleus, whereas CT-longQ27 is targeted to the cytoplasm and nucleus in HEK293 cells. HEK293 cells were transfected with CT-short or

and holding potential of 0 mV. All measurements of intrinsic firing properties were made at 35°C bath temperature. A combination of EPC10/2 amplifier and PatchMaster software (HEKA Elektronik) was used to control membrane voltage, stimulation timing, and data acquisition. Series resistance was compensated routinely by 70–80%. Membrane currents were filtered at 3 kHz and digitized at 20 kHz.

#### Extracellular in vivo recordings of PCs

Recordings have been performed as described previously (Krause et al., 2014). Briefly, adult mice (one males and two females for floxed (fl)-CT-short; three males for CT-short<sup>PC</sup>; three males for fl-CT-longQ27; and three males for CT-longQ27<sup>PC</sup>) were anesthetized with an intraperitoneal injection of ketamine (10 mg/kg)/xylazine (20 mg/kg), with supplemental ketamine doses during the experiment. After placing the mice in a stereotaxic frame (Narishige), a sagittal incision was performed along the midline to expose the cranium and a window 6 mm caudal from bregma to give access to the vermis. A multielectrode device (Eckhorn microdrive; Thomas Recording) was used to monitor single PCs.

Single-cell activity was sampled with high temporal resolution (32 kHz) and analyzed offline for spike detection. Alternatively, signals of multiple electrodes were routed through an online spike sorter (Plexon), and time markers for each detected action potential was stored. Throughout the experiments, PCs were identified by the combined occurrence of simple and complex spikes. Complex spikes can only be detected in PCs and represent the climbing fiber input into PCs (Schmolesky et al., 2002).

←  
CT-longQ27 and incubated for 14–20 h at 37°C. **B<sub>1</sub>**, Phase-contrast and DAPI and YFP fluorescence (bottom) images of transfected HEK293 cells. **B<sub>2</sub>**, xyz images of the cells shown in **B<sub>1</sub>** demonstrates that CT-short formed nuclear aggregates that are larger in size compared with nuclear and cytoplasmic CT-longQ27 formed aggregates. **B<sub>3</sub>**, Bar graph of the fluorescence distribution of CTs between the nuclear and non-nuclear region of the cell. Cell borders were identified by the phase-contrast image, whereas nuclear regions were defined by the DAPI staining. The diagram shows that >90% of the YFP fluorescence of CT-short is found in the nucleus, whereas 50–60% of the CT-longQ27 YFP fluorescence is outside of the nuclear areas. **B<sub>4</sub>**, Diagram of the size of CT-containing aggregates reveal that CT-short forms larger aggregates than CT-longQ27. Statistical significance was evaluated with ANOVA (\* $p < 0.05$ , \*\* $p < 0.01$ ). Error bars indicate SEM. **C**, CT-short is targeted predominantly to the nucleus, whereas CT-longQ27 is found predominantly in cytoplasmic aggregates in cerebellar PCs. AAV2-mediated expression of CT-short and CT-longQ27 in cerebellar PCs 3–4 weeks after injection into 2- to 3-week-old mice. **C<sub>1</sub>**, CT-short is found in large nuclear aggregates and distributed diffusely in some of the proximal dendrites. CT-longQ27 is found in small aggregates in the soma and in particular in the dendrites of PCs. **C<sub>2</sub>**, **C<sub>3</sub>**, Number of PCs expressing CT-short (**C<sub>2</sub>**) or CT-longQ27 (**C<sub>3</sub>**) that reveal a punctate distribution in the cytoplasm or a diffuse or punctate distribution in dendrites. Statistical significance was evaluated with ANOVA (\*\* $p < 0.01$ ). Error bars indicate SEM.

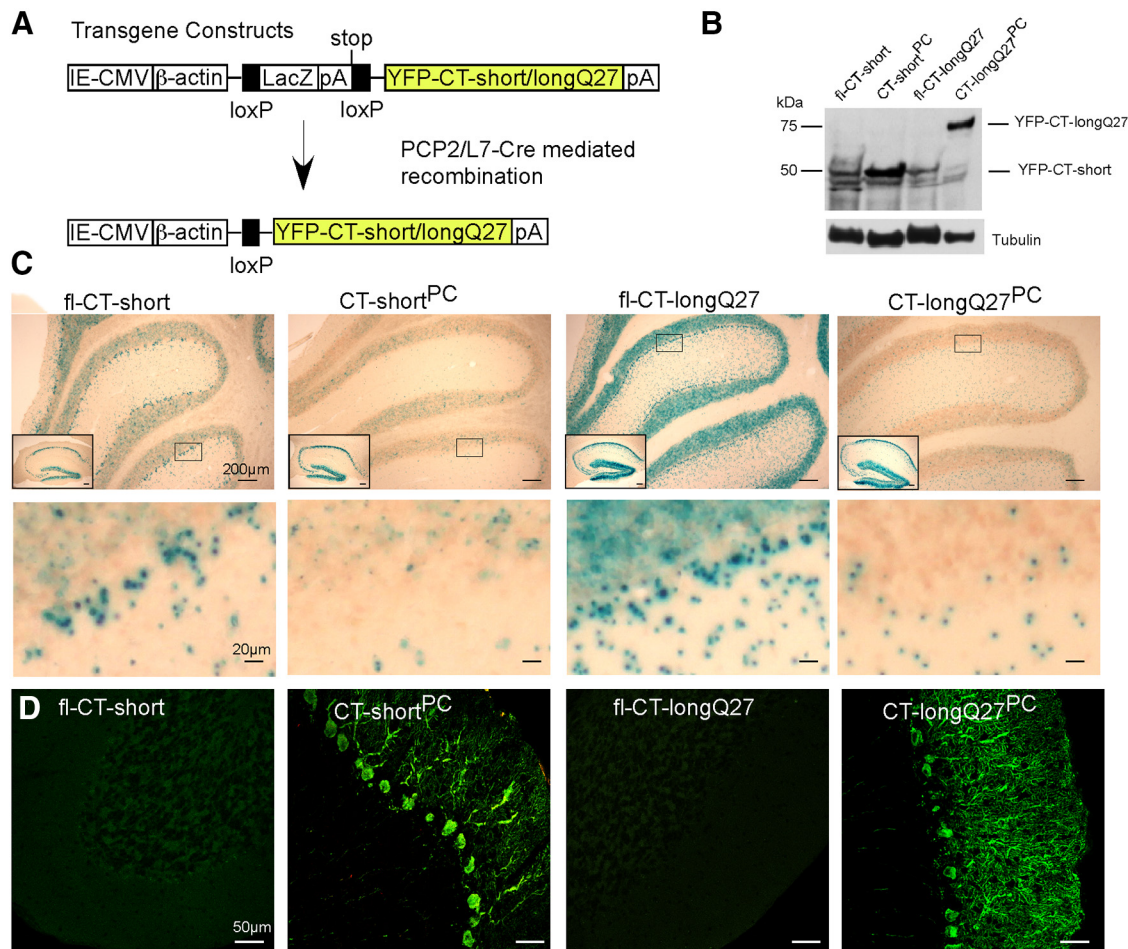


**Figure 2.** Floxed CT peptide expressing mice for cell-type-specific Cre recombinase-mediated expression and characterization of CT-short and CT-longQ27 in PCs of the cerebellum. **A**, Schematic description of the constructs used to create the transgenic animals expressing CT-short (fl-CT-short) or CT-longQ27 (fl-CT-longQ27). CT-short and CT-longQ27 were both cloned into pCZW (Braz et al., 2002), which contains a CMV and  $\beta$ -actin promoter and a lacZ expression cassette that is flanked with loxP sequences. After Cre-mediated recombination, the lacZ expression cassette is excised out, resulting in mice (CT-short<sup>PC</sup> and CT-longQ27<sup>PC</sup>) expressing the CTs only in the cell types containing the Cre recombinase. polyA, Polyadenylation. **B**, Western blot analysis of cerebellar homogenates from adult mouse brains expressing YFP-CT-short and YFP-CT-longQ27 specifically in PCs. YFP-CT-short and YFP-CT-longQ27 were detected using a GFP antibody, and  $\alpha$ -tubulin was used as a loading control. No differences were detected in the expression levels between YFP-CT-short- and YFP-CT-longQ27-expressing mice. **C**, LacZ expression in fl-CT-short and fl-CT-longQ27 mice and Cre recombinase-induced expression of CT-short<sup>PC</sup> and CT-longQ27<sup>PC</sup> in PCs (arrows show PC layer) of the cerebellum. Cerebellar sagittal sections from fl-CT-short and fl-CT-longQ27 adult mice reveal  $\beta$ -gal staining in cerebellar PCs (bottom) and the hippocampus (inset; top). PC-specific expression of Cre recombinase in CT-short<sup>PC</sup> and CT-longQ27<sup>PC</sup> mouse lines resulted in a loss of  $\beta$ -gal staining in PCs (bottom) but not in hippocampus (inset; top) and a gain of YFP-CT-short and YFP-CT-longQ27 expression in PCs (**D**). YFP was visualized with a GFP antibody in cerebellar sagittal sections from adult mice.

**Creation of transgenic animals and transgene detection**

For stable integration of Ca<sup>2+</sup> channel constructs into the mouse genome, the human CT-short and CT-longQ27 was cloned into pCZW (Braz et al., 2002). pCZW contains the ubiquitous CMV/ $\beta$ -actin promoter from chicken and a lacZ expression cassette that is flanked with loxP sequences. In these mice, CT expression can be activated by the excision of  $\beta$ -galactosidase ( $\beta$ -gal) encoding DNA by Cre recombinase. The cDNA of  $\beta$ -gal was inserted before the start codon flanked by loxP sequences. Expression of Cre recombinase in the tissue or neuronal population of choice allows the expression of the CT. Additionally, we inserted a YFP tag 5' of the CT construct for determining the protein expression of the constructs. The pCZW-YFP-CT-short and pCZW-YFP-CT-longQ27 constructs were microinjected into the mice by the Case Western Reserve University Transgenic Core Facility (Cleveland, OH).

Transgene expression was detected by PCR analysis (forward, 5' CGACCCTACCAGCAGAACA 3'; reverse, 5' CCACGGACTGAGAGTTAGGC 3') and  $\beta$ -gal staining. Three male mice of >8 weeks of age were perfused, allowing for adequate time for expression of the transgene. Mice were perfused with 4% paraformaldehyde in PBS, pH 7.4 (Electron Microscopy Science), and dissected brains were postfixed in the same solution for 1 h. 5-Bromo-4-chloro-3-indolyl- $\beta$ -D-glucuronidase

(X-gal) staining and immunohistochemistry were performed according to the methods of Xu et al. (2006). Tissues have been placed in 30% sucrose (w/v) and 1 $\times$  PBS overnight at 4°C and sectioned sagittally on a cryostat at 30  $\mu$ m. For immunohistochemistry, sagittal brain slices from at least three male mice per genotype were stained with a primary antibody against GFP (1:500 dilution; Frontier Institute) and conjugated with goat anti-rabbit Alexa Fluor 488 secondary antibody (1:1000; Invitrogen). Fluorescence was monitored under an Olympus fluorescence microscope. For X-gal staining, sagittal brain slices were washed three times for 10 min in PBS plus 0.2% Triton X-100. X-gal (40 mg/ml; Roche) was dissolved into N,N-dimethylformamide (Sigma). Brain sections were incubated with 0.25 ml of staining solution composed of 5 mM K3Fe(CN)6, 5 mM K4Fe(CN)6, 2 mM MgCl<sub>2</sub>, and 1 mg/ml X-gal in 1 $\times$  PBS at 37°C overnight. The slices were examined under a light microscope for X-gal development and photographed on a Spot RT-Color Diagnostic digital camera.

Positive selected founders that showed high  $\beta$ -gal expression in PCs were expanded and analyzed for the expression and function of human CTs. To activate the expression of CTs, transgenic lines were crossbred with mice that express Cre recombinase specifically in PCs. The mouse line Tg(Pcp2-cre)1Amc/J (Barski et al., 2000) expresses Cre recombi-

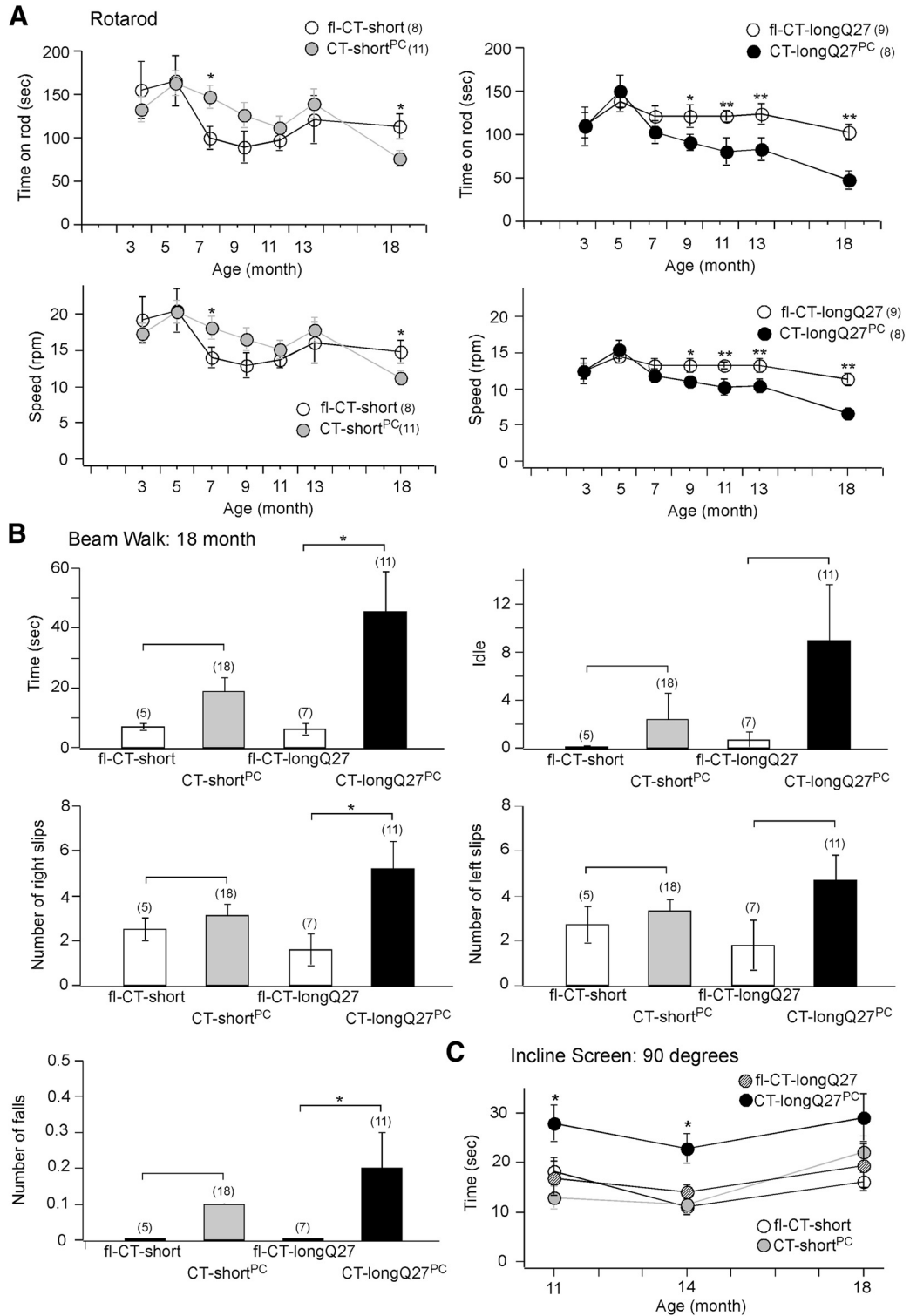


**Figure 3.** Behavior analyses of CT-short<sup>PC</sup> and CT-longQ27<sup>PC</sup> mice. Comparisons between CT-short<sup>PC</sup> and CT-longQ27<sup>PC</sup> and fl-CT-short and fl-CT-longQ27 control mice on rotarod (A), beam-walk (B), and incline screen (C) tests. Statistical significance in all behavior experiments was evaluated with ANOVA. \**p* ≤ 0.05, \*\**p* ≤ 0.01. Data are reported as mean ± SEM. The number in parentheses indicates the number of animals tested.

nase under the PC-specific Pcp2/L7 promoter. The Pcp2 promoter is a widely used promoter for driving PC-specific expression. Expression of transgenes under this promoter can be first detected at postnatal day 6 and full expression after postnatal week 2–3 (Barski et al., 2000). Because the promoter is not active early in development, we did not see any developmental problems related to the transgene expression in previous studies (Mark et al., 2011).

Western blots from three adult male age-matched fl-CT-short, fl-CT-longQ27, CT-short<sup>PC</sup>, and CT-longQ27<sup>PC</sup> mouse brain homogenates were performed according to the methods of Han et al. (2006). The cerebellum from at least three adult male mice per genotype were analyzed. Detection of YFP constructs with anti-GFP (1:1000; Frontier Institute), followed by a secondary horseradish peroxidase antibody (1:5000; Pierce) was used. The blots were stripped with a mild stripping buffer (Abcam) and reincu-

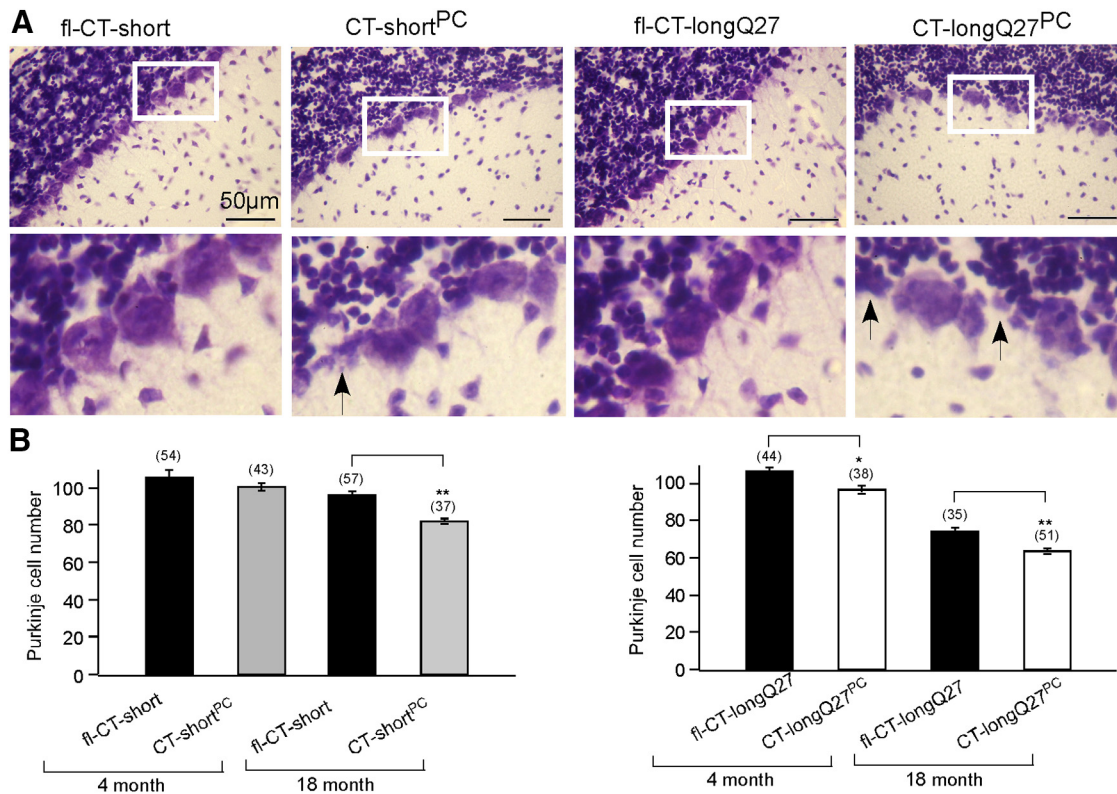


**Figure 4.** Degeneration of PCs with age in CT-short<sup>PC</sup> and CT-longQ27<sup>PC</sup> mice. **A**, Representative images of the PC layer in cerebellar slices from 18-month-old CT-short<sup>PC</sup> and CT-longQ27<sup>PC</sup> mice. Arrows show missing PCs. **B**, Quantification of the number of PCs per area in cerebellar slices for 4- and 18-month-old CT-short<sup>PC</sup> and CT-longQ27<sup>PC</sup> mice. Statistical significance was evaluated with ANOVA (\* $p < 0.05$ , \*\* $p < 0.01$ ). Error bars indicate SEM.

bated with an anti- $\alpha$ -tubulin antibody (1:1000; Thermo Fisher Scientific) as a loading control. Blots were developed according to the SuperSignal West Dura Extended Duration Substrate protocols (Pierce).

**Analysis of ataxic behavior**

Analysis of ataxic behavior has been described in detail previously (Mark et al., 2011; Maejima et al., 2013) and briefly below.

**Rotarod.** Mice (four males and four females for fl-CT-short; six males and five females for CT-short<sup>PC</sup>; four males and five females for fl-CT-longQ27; and four males and four females for CT-longQ27<sup>PC</sup>) were placed on a rotarod (Columbus Instruments) rotating at 4 rpm for 1 min of acclimation. The rod was then accelerated at 0.1 rpm/s up to 40.0 rpm. The test continued until all mice had fallen off the rod. Latency to fall and rotations per minute at the time of fall were recorded for each mouse. Data were averaged over three trials per mouse.

**Incline screen test.** Two wire mesh screens, one at a 60° angle and the other at a 90° angle, were used for this test. Mice (two males and three females for fl-CT-short; 10 males and eight females for CT-short<sup>PC</sup>; three males and four females for fl-CT-longQ27; and six males and five females for CT-longQ27<sup>PC</sup>) were placed facing downward in the middle of the screen. Latency to turn around and climb to the top was recorded. Maximum latency to complete the task was set at 60 s. If the mouse fell, a time of 60 s and a fall notation were recorded.

**Beam walk.** Mice (two males and three females for fl-CT-short; 10 males and eight females for CT-short<sup>PC</sup>; three males and four females for fl-CT-longQ27; and six males and five females for CT-longQ27<sup>PC</sup>) were analyzed for their capability to cross a narrow beam to an enclosed goal box. The horizontally placed, 70-cm-long beam was 10 mm wide and 60 cm above the table surface. One end of the beam was mounted to a small, illuminated platform, and the other end was fastened to an enclosed (15 cm<sup>2</sup>) goal box. Mice underwent training for 2 d (six trials per day) before data collection. Briefly, the mouse was placed at an illuminated end of the beam, and the time required to traverse the beam to the goal house was recorded. Mice were given a maximum of 120 s to transverse the beam, and a fall was

also recorded as 120 s. In addition to recording the latency to transverse the beam, time spent immobile (idle), left and right paw slips, and falls were noted (Quinn et al., 2007). Data were averaged over three trials per mouse.

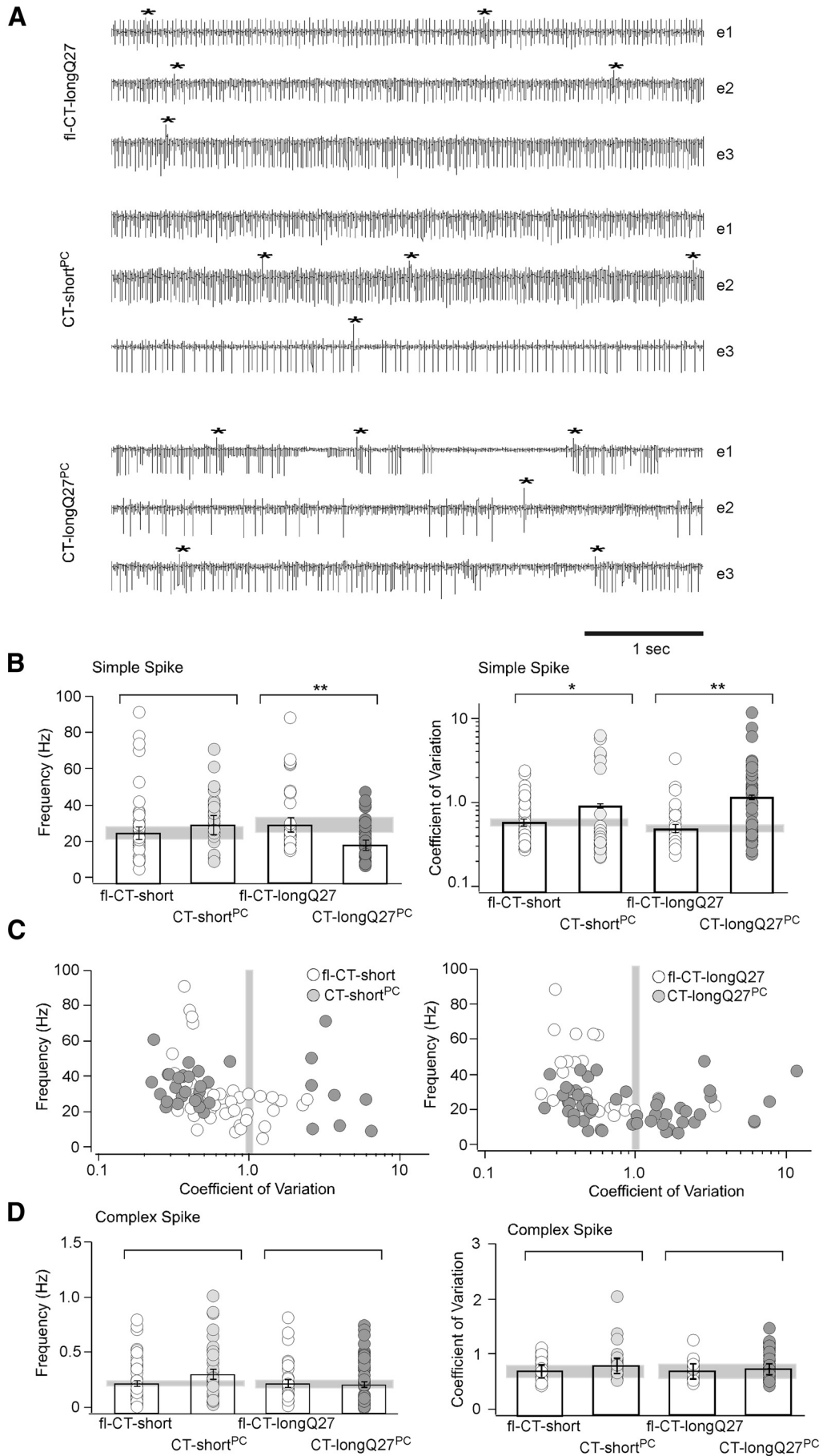
**EBC**

EBC was performed as described previously (Koekkoek et al., 2002; Boele et al., 2013). Briefly, at least four age-matched (6–8 months old) male mice underwent a 3 d habituation (one session per day), followed by a 6 d training and 3 d extinction period. Animals were housed in their home cage until the start of each session. EBC experiments were performed in an isolated training box (Blink2.0; Neurasmus). Animals were placed inside of a slow rotating wheel to keep the mice alert during the sessions. Before the start of the habituation session, the minimal tone intensity that did not induce a startle response was determined (~70 dB). A sinusoidal tone with a duration of 380 ms (rise/fall time 25 ms) and a frequency of 5 kHz were used as the conditioning stimuli (CS). The unconditioned stimuli (US) consisted of a 30-ms-long mild air puff to the cornea of the eye. In the training session, the CS was paired with the US with an interstimulus interval of 350 ms. During each session, animals received 64 trials in eight blocks. Each block consisted of one US, followed by six paired CS-US, followed by one CS, with each stimuli separated by a random inter-trial interval of 30 s ( $\pm 10$  s). Eyelid movements were monitored with the magnetic distance measurement technique (MDMT; Koekkoek et al., 2002). A magnetosensitive chip placed above the upper eyelid detects the movement of a magnet that has been placed on the lower eyelid of the mice before the recording session. During the habituation and extinction sessions, the blocks consisted of randomly paired US-only and CS-only trials. All experiments were approved by the Institutional Animal Research Facility.

**Results**

**CT-short forms mainly nuclear inclusions, whereas CT-long forms mainly cytoplasmic aggregates in HEK293 cells and cerebellar PCs**

PolyQ diseases are characterized by protein aggregations within the nucleus (nuclear inclusions) and cytoplasm (cytoplasmic ag-



gregates). Interestingly, SCA6 patients reveal cytoplasmic aggregates with few nuclear inclusions found in cerebellar neurons (Ishikawa et al., 1999b, 2001; Koepfen, 2005). Recently, Kordasiewicz et al. (2006) demonstrated that the CT of the P/Q-type channel is located within the nucleus of mouse and human PCs (Kordasiewicz et al., 2006). Because the CT of the  $\text{Ca}_v\alpha_12.1$  subunit has been identified as a proteolytic and/or transcriptional product of the channel (Kubodera et al., 2003; Kordasiewicz et al., 2006; Du et al., 2013), we analyzed how the 60–75 kDa CT peptide of the P/Q-type channel  $\text{Ca}_v\alpha_1$  subunit might be involved in the early and late phase of the SCA6 disease. We first examined the distribution of two CT constructs in HEK293 cells. These constructs were the short CT without exon 47 (CT-short) and the long CT [including exon 47, i.e., CT with 27 Gln (Qs) (CT-longQ27, “disease form”; Fig. 1A)]. The YFP-tagged CTs showed a distinct pattern of expression with CT-short distributing predominantly to the nucleus and forming large, immobile nuclear inclusions (Fig. 1B). CT-longQ27 distributed to the nucleus and the cytosol, in which they formed mobile inclusions (Fig. 1B). We found three patterns of CT-longQ27 distribution, i.e., cells with exclusive nuclear aggregates, cells that revealed nuclear and cytoplasmic aggregates, and cells that only had cytoplasmic aggregates. For all CT-longQ27-expressing cells, the inclusions were consistently of smaller size and number (Fig. 1B<sub>4</sub>).

To analyze the distribution and physiological function of the CT peptides in PCs, we stereotactically injected AAV2 expressing the different CT peptides under the control of the CMV promoter into the cerebellar cortex of 2- to 3-week-old mice and detected fluorescent staining after 2–3 weeks of expression mainly in PCs (70% PCs, 23% granule cells, and 7% other cells; data not shown). As observed in HEK293 cells, CT-short mainly distributed to the nucleus to form large aggregates. In 20% of the PCs, CT-short also diffused into the cytoplasm of the proximal dendrites without forming aggregates (Fig. 1C). In contrast, CT-longQ27 was found in nuclear and cytoplasmic aggregates around the soma and revealed a clustered distribution particularly in distal dendrites (Fig. 1C). Thus, CT-short and CT-longQ27 reveal nuclear and cytoplasmic aggregates as found in SCA6 patients.

### Characterization of the functional consequences of CT-short and CT-longQ27 expression in the cerebellar cortex

To analyze the physiological and behavioral consequences of expression of the two CT splice variants found in the cerebellum of

←

**Figure 5.** *In vivo* PC recordings from CT-short<sup>PC</sup> and CT-longQ27<sup>PC</sup> mice. **A**, Three simultaneous recordings from a control fl-CT-longQ27 (top), CT-short<sup>PC</sup> (middle), and CT-longQ27<sup>PC</sup> (bottom) mouse. All recordings are representative of a single PC, as demonstrated by a pause in simple spikes after occurrence of a complex spike (marked with asterisks). Simple spikes from additional putative PCs are evident in electrodes e2 and e3 in the bottom. Note the regular simple spike firing in the control fl-CT-longQ27 and majority of CT-short<sup>PC</sup> recordings. In CT-longQ27<sup>PC</sup> mice, simple spikes fire more irregularly with intermittent pauses that occur independently at different PCs. **B**, In CT-longQ27<sup>PC</sup> mice, simple spike firing is significantly reduced, whereas CT-short<sup>PC</sup> PCs do not differ in firing rate from their control fl-CT-short littermates. The CV from interspike intervals are higher in CT-short<sup>PC</sup> and CT-longQ27<sup>PC</sup> mice, which suggests less regular firing in these mice. **C**, Scatter plots of simple spike frequency versus CV indicate subpopulations of cells in CT-short<sup>PC</sup> and CT-longQ27<sup>PC</sup> mice with either CVs <1 (CT-short<sup>PC</sup>, 26 of 34 = 76.5%; CT-longQ27<sup>PC</sup>, 28 of 51 = 54.9%) or CVs >1 (CT-short<sup>PC</sup>, 8 of 34 = 23.5%; CT-longQ27<sup>PC</sup>, 23 of 51 = 45.1%), whereas in both control groups, there is a higher percentage of regular firing cells with CVs <1 (fl-CT-short, 83.0%; fl-CT-longQ27, 90.9%). Continuous-spiking PCs (CV <1) with spike rates >50 Hz are restricted mostly to the control mice. **D**, The CTs had no significant effect on the spike frequency and CVs from complex spikes in the different mouse lines; \* $p < 0.05$ , \*\* $p < 0.01$ .

SCA6 patients, we created two transgenic mouse lines (fl-CT-short and fl-CT-longQ27) for cerebellar expression of these constructs specifically in PCs using the Cre-lox system (Fig. 2A). Crossing the floxed CT-expressing mice with a mouse line that expresses Cre recombinase specifically in PCs ( $\text{Tg}^{\text{PCP2-Cre}}$ ; Barski et al., 2000) resulted in PC-specific expression of CT peptides beginning 1–3 weeks after birth (Fig. 2B–D; Mark et al., 2011). These mice expressing the CTs specifically in PCs of the cerebellum will be referred to as CT-short<sup>PC</sup> and CT-longQ27<sup>PC</sup>. No differences in the amount of CT protein expression was found between the CT-short<sup>PC</sup>- and CT-longQ27<sup>PC</sup>-expressing mice (Fig. 2B,D).

### Postnatal expression of CT-longQ27<sup>PC</sup> but not CT-short<sup>PC</sup> causes ataxia and alteration in the firing properties of PCs *in vivo*

SCA6 patients are characterized by late-onset ataxia and degeneration of cerebellar PCs. Therefore, we analyzed motor behavior of CT-short<sup>PC</sup>- and CT-longQ27<sup>PC</sup>-expressing mice. We found that CT-longQ27<sup>PC</sup>-expressing mice develop signs of ataxia beginning at 8 months of age when tested on the rotarod (Fig. 3A). Rotarod performance declined further with age (Fig. 3A). Impairment of motor performance became also obvious in the incline screen test and the beam-walk test (Fig. 3B,C). In contrast, CT-short<sup>PC</sup>-expressing mice developed late signs of ataxia only after 18 months of age and only on the rotarod but not on the incline screen or beam-walk tests (Fig. 3A–C). Both mouse lines showed an age-dependent reduction in the number of PCs. However, reduction in PC number occurred much earlier in CT-longQ27<sup>PC</sup> (after 4 months) compared with CT-short<sup>PC</sup> (after 18 months)-expressing mice (Fig. 4).

Ataxia is most likely caused by an alteration in the information processing and output signals of the cerebellar cortex because of either neuronal degeneration (see above) or changes in the information processing of PCs before neuronal death. Therefore, we analyzed to what extent expression of CT peptides interferes with the firing properties of PCs *in vivo*.

Indeed, simultaneous multiple electrode recordings revealed more irregular simple spike firing in CT-longQ27<sup>PC</sup> compared with CT-short<sup>PC</sup> and control mice. The intermittent firing was not a ubiquitous and/or continuous feature of all PCs in CT-longQ27<sup>PC</sup> mice, because we sometimes recorded intermittently firing PCs together with regularly firing PCs. When multiple PCs with irregular firing were recorded in parallel, pauses in simple spike firing appeared independently at different cells with no indication of temporal coupling of pauses in different PCs (Fig. 5A, bottom). The mean frequency of simple spike firing was reduced significantly in CT-longQ27<sup>PC</sup> (Fig. 5B, left), which is probably a direct consequence of occurrence of pauses in simple spike trains. The simple spike irregularity, quantified by the coefficient of variation (CV) of the interspike interval distribution, was increased in both CT-short<sup>PC</sup> and CT-longQ27<sup>PC</sup> when compared with control mice (CT-short, CV = 1.20 vs 0.74,  $p < 0.05$ ; CT-longQ27<sup>PC</sup>, CV = 1.62 vs 0.61,  $p < 0.01$ ; Fig. 4B<sub>4</sub>, right).

The results on simple spike firing frequency and CV suggest that CT-longQ27<sup>PC</sup> mice have a higher incidence of irregular firing cells compared with CT-short<sup>PC</sup> and control mice. To distinguish regularly from intermittently firing PCs, we plotted the simple spike rate versus the CV values. Regularly firing PCs might form a cluster with CVs <1 and higher rates compared with irregularly firing PCs that are characterized by CVs >1 and lower rates (Yartsev et al., 2009). The scatter plot revealed that CT-short<sup>PC</sup> and CT-longQ27<sup>PC</sup> show two subpopulations of PCs

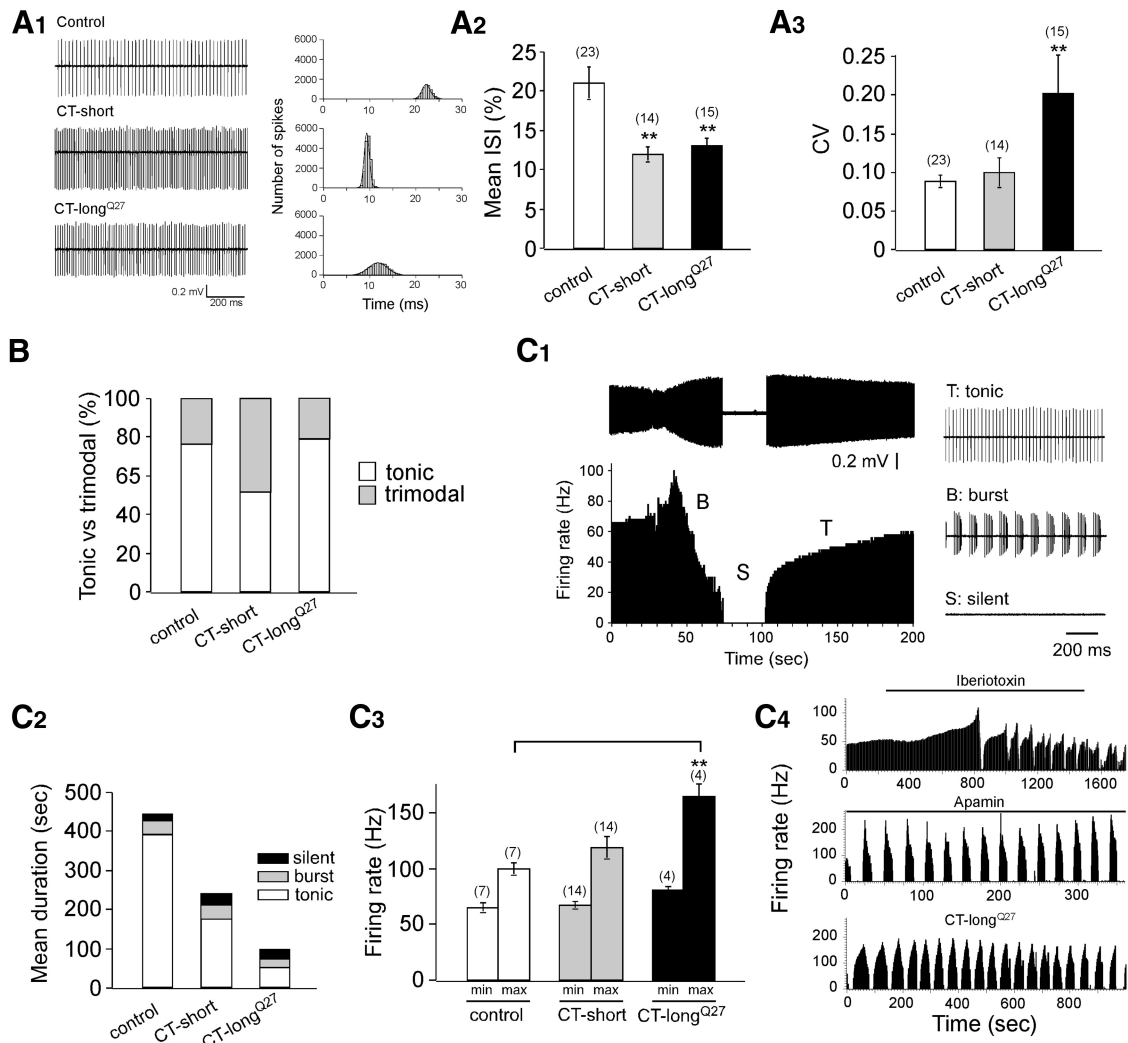


**Figure 6.** Action potential firing patterns from virally expressed CT-short and CT-longQ27 cerebellar PCs. **A**, Analysis of tonically firing PCs. **A**<sub>1</sub>, Example trace of extracellular action potential recordings of CT-short- and CT-longQ27-expressing or control PCs. **A**<sub>2</sub>, Firing rate of CT-short- and CT-longQ27-expressing or control PCs. **A**<sub>3</sub>, CVs of the mean firing rate from CT-short- and CT-longQ27-expressing or control PCs. **B**, Percentage of recorded control or CT-short- or CT-longQ27-expressing PCs with tonic or trimodal firing patterns. **C**, Analysis of trimodal firing of PCs. **C**<sub>1</sub>, Example trace of extracellular action potential recordings of a control PC in the trimodal phase illustrating the tonic, bursting and silent phase. **C**<sub>2</sub>, Duration of the trimodal firing cycle with duration for each firing phase for CT-short- and CT-longQ27-expressing or control PCs. **C**<sub>3</sub>, Maximum firing rates during the trimodal phase of CT-short- and CT-longQ27-expressing or control PCs. **C**<sub>4</sub>, Comparison of repetitive trimodal firing for CT-longQ27-expressing PCs (bottom) with control PCs after application of 100 nM BK channel blocker iberiotoxin (top) or 100 nM SK channel blocker apamin (middle).

when  $CV = 1$  is used as a threshold (Fig. 5C). Accordingly, the incidence of intermittent firing cells ( $CV > 1$ ) was highest in CT-longQ27<sup>PC</sup> (23 of 51 PCs = 45.1%, three mice, 17.1–28.9 months) compared with 23.5% (8 of 34 cells) in CT-short<sup>PC</sup> mice ( $n = 3$ , 16.1–33.9 months) and 9.1% (3 of 33) in fl-CT-longQ27 (control, three mice, 13.5–16.7 months) and 17.0% (8 of 47) in fl-CT-short mice (control,  $n = 3$ , 16.1–32.6 month). No differences were observed in the rates and regularity of complex spikes (Fig. 5D). Thus, the data suggest that PCs expressing CT-longQ27<sup>PC</sup> mice reveal a higher incidence of irregular firing. The CV for adjacent intervals (CV2) did not reveal significant differences between CT-short<sup>PC</sup> and CT-longQ27<sup>PC</sup>. This indicates that the variability in the simple spike firing in CT-longQ27<sup>PC</sup> is generated by slow modulations and longer pauses in firing that have a significant influence on the CV measure but weak influence on CV2.

Next we wanted to investigate the effects AAV2-expressing CTs (CT-short and CT-longQ27) on the spontaneous firing of

PCs in the presence of synaptic transmission blockers. To accomplish this, we stereotactically injected AAV2-expressing CTs in 3- to 4-week-old mice and recorded 10–14 d later from positively expressing PCs in cerebellar slices. Spontaneously active PCs in cerebellar slices revealed either a tonic or a trimodal firing pattern, possibly reflecting enhanced bistability or tristability (Schonewille et al., 2006). PCs in the trimodal firing state cycled continuously among a silent, tonically active and bursting phase (Womack and Khodakhah, 2002; Fig. 6C<sub>1</sub>). We first analyzed tonically firing PCs and found that expression of CT-short and CT-longQ27 revealed a reduction in the firing frequency (Fig. 6A<sub>2</sub>). PCs expressing CT-longQ27-expressing PCs fire more irregularly compared with CT-short-expressing PCs as suggested by the higher CV (CT-short,  $CV = 0.10 \pm 0.02$ ; CT-longQ27,  $CV = 0.203 \pm 0.049$ ; Fig. 6A<sub>3</sub>). We observed more PCs expressing CT-short in the trimodal state compared with control and CT-longQ27-expressing PCs, whereas more PCs expressing CT-longQ27 appeared in the silent mode (putative downstate;

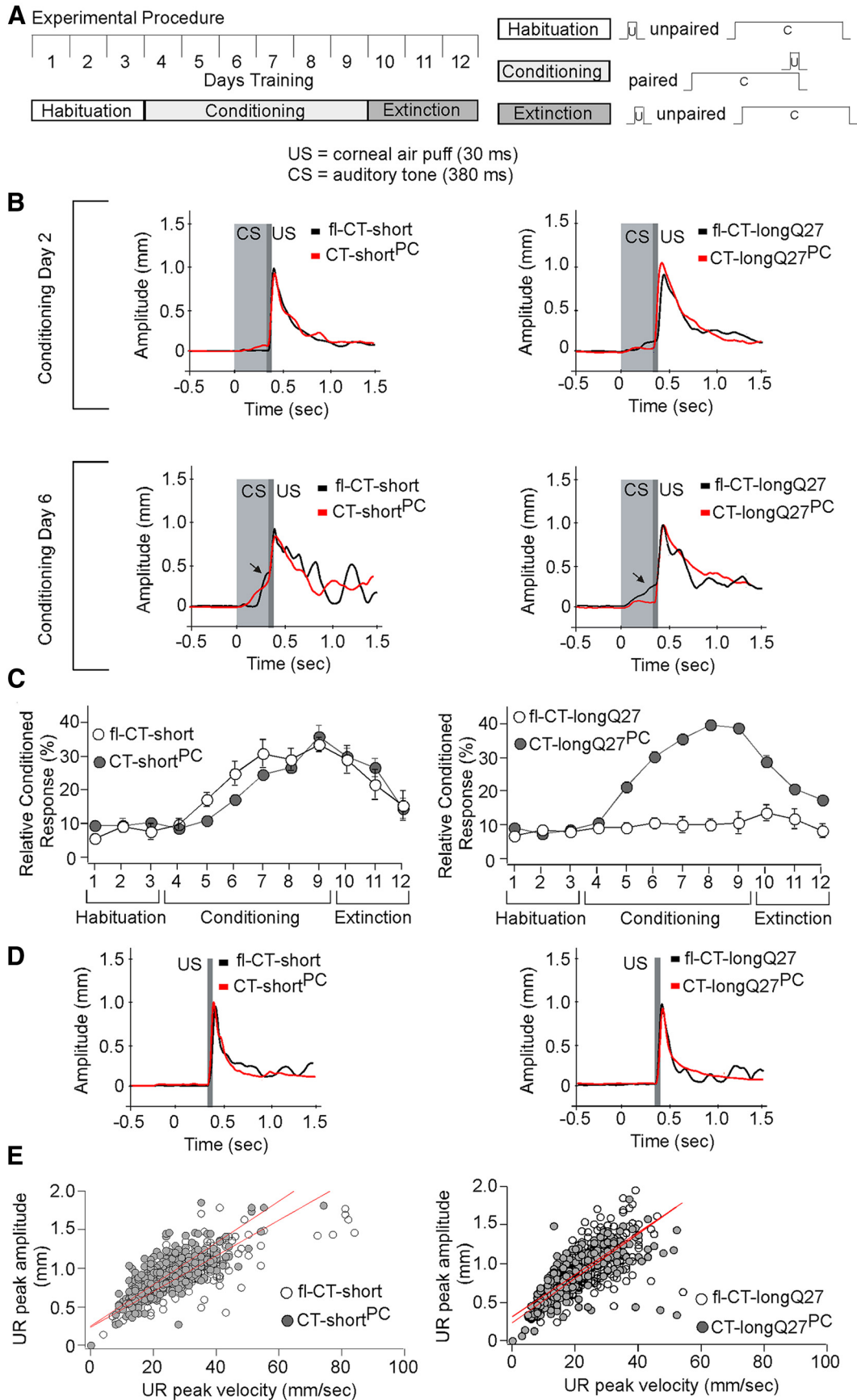


**Figure 7.** EBC in CT-short<sup>PC</sup> and CT-longQ27<sup>PC</sup> mice. **A**, Schematic diagram of the experimental procedure used for analyzing the EBC in mice. Left, Animals underwent a 12 d behavioral assay with three sessions of habituation, six sessions of conditional learning, and three sessions of extinction with one session per day. The US was a 30 ms mild corneal air puff; the CS was a 380-ms-long auditory tone. Right, For habituation, a US was elicited randomly before the CS. For conditioning, the US was elicited at the end of the CS. For extinction the US (Figure legend continues.)

Schonewille et al., 2006). Additionally, PCs expressing CT-short and CT-longQ27 showed a reduced mean duration of the tonic state from  $173.6 \pm 24.5$  s for CT-short and  $49.7 \pm 2.3$  s for CT-longQ27 in the trimodal state (Fig. 6C<sub>2</sub>). The drastic reduction in the mean duration of the tonic phase in CT-longQ27-expressing PCs was accompanied by an increase in the maximal firing rate (Fig. 6C<sub>3</sub>). An increase in trimodal cycle time and maximal firing frequency has also been observed when SK channels, i.e., Ca<sup>2+</sup>-activated K<sup>+</sup> channels, are blocked in PCs (Womack and Khodakhah, 2003). Therefore, we compared the trimodal firing pattern and firing frequency between CT-longQ27-expressing PCs and PCs in which SK channels are blocked. Indeed, SK channel block leads to a similar, but more pronounced, change in trimodal firing as observed for CT-longQ27-expressing PCs (Fig. 6C<sub>4</sub>), suggesting that CT-longQ27 may interfere with the interaction between P/Q-type channels and SK channels (Womack et al., 2004; Indriati et al., 2013).

Postnatal expression of CT-longQ27<sup>PC</sup>, but not CT-short<sup>PC</sup>, impairs EBC and cerebellar plasticity at the PF–PC synapse. EBC is a form of associative learning that requires precise information processing within the cerebellar cortex (Kim and Thompson, 1997; De Zeeuw et al., 2011). For example, lesions in defined cerebellar areas in human patients lead to deficits in timing, acquisition, and extinction of eyeblink responses (Gerwig et al., 2007), and changes in synaptic plasticity of the cerebellar cortex impairs EBC (Koekkoek et al., 2003; Schonewille et al., 2010, 2011). To examine changes in EBC caused by the presence of CTs, we analyzed EBC responses in CT-short<sup>PC</sup>, CT-longQ27<sup>PC</sup>, and control (fl-CT-short, fl-CT-longQ27) mice using an MDMT (Koekkoek et al., 2002). Closing of the eyelid is induced by a corneal air puff (the US) and is associated timely during a 6 d training session with a CS, i.e., an auditory tone (Fig. 7A). As shown in Figure 7B, we found that in CT-longQ27<sup>PC</sup> mice EBC responses are suppressed almost completely during the 6 d training period, whereas EBC responses in CT-short<sup>PC</sup> mice are comparable with control mice.

Because changes in synaptic plasticity at the PF–PC synapse may impair EBC responses (Koekkoek et al., 2003; Schonewille et al., 2010, 2011), we analyzed whether LTD and LTP were affected in cerebellar slices in the presence or absence of CT peptides using whole-cell patch-clamp recordings after AAV2 expression. Indeed, we found that virally expressed CT-longQ27, but not CT-short, suppresses both LTD (Fig. 8A,B) and LTP (Fig. 8C,D) at the PF–PC synapse.

## Discussion

PolyQ extension within the P/Q-type channel CT has only minor effects on gating and Ca<sup>2+</sup> permeability (Saegusa et al., 2007;

←

(Figure legend continued.) was again randomly elicited before the CS. **B**, Averaged traces of paired CS–US trials from CT-short<sup>PC</sup> (left, red) and CT-longQ27<sup>PC</sup> (right, red) compared with their respective control mice, fl-CT-short and fl-CT-longQ27 (black) at conditioning day 2 (top) and conditioning day 6 (bottom). The arrow indicates the conditioning response (partial eyelid closure) at the end phase of the CS (light gray bar). The US occurs 350 ms after the CS onset (dark gray bar). SDs were not shown for clarity reasons. **C**, Learning curves: percentage of conditioned eyelid responses relative to all trials during habituation, conditioning, and extinction during the 12 d behavioral assay for CT-short<sup>PC</sup> (left), CT-longQ27<sup>PC</sup> (right), and control mice. **D**, Example traces of US trials from CT-short<sup>PC</sup> (left, red) and CT-longQ27<sup>PC</sup> (right, red) mice compared with their control mice (black) demonstrate that the US-induced eyelid responses are not different between CT-short<sup>PC</sup>, CT-longQ27<sup>PC</sup>, and control mice. **E**, Plot of the peak amplitude of the unconditioned response in relation to the peak velocity of the unconditioned response demonstrates that the kinetics of the eyelid responses are not perturbed in CT-short<sup>PC</sup> and CT-longQ27<sup>PC</sup> mice compared with control mice.

Watase et al., 2008). Thus, a change in the biophysical properties of the channel may have only a small contribution to the disease phenotypes (Orr, 2012). After detection of the P/Q-type channel CTs in PCs from SCA6 patients (Ishiguro et al., 2010), it has been suggested that a CT peptide fragment might be the cause of the disease. The CT peptide fragments seem to be produced by either proteolytic processing (Kubodera et al., 2003; Kordasiewicz et al., 2006) or translation from a bicistronic mRNA (Du et al., 2013). Indeed, because they are localized in the cytoplasm and nuclei of PCs, they may interfere with the function of proteins in PCs and/or change their gene expression. Regardless of whether CT-longQ<sub>(disease)</sub> is produced via proteolytic processing or via its own transcriptional start site, CT-longQ<sub>(disease)</sub> has been shown to be toxic to cells in cultures and to cause cell death for PCs *in vivo* (Kordasiewicz et al., 2006; Du et al., 2013; Takahashi et al., 2013). Therefore, we were interested in establishing an animal model and viral techniques to analyze the physiological function of the two CT fragments, i.e., CT-short and CT-longQ27 for disease phenotypes. These two CT variants are present in the human cerebellum by the identified P/Q-type channel splice variants. Here, 65% of P/Q-type channel mRNA consists of the long form, whereas 35% consist of the short form (Soong et al., 2002). The ratio of the long (toxic) form of Ca<sub>v</sub>2.1 mRNA compared with total Ca<sub>v</sub>2.1 mRNA in cerebellar PCs of SCA6 patients ( $0.98 \pm 0.06$ ) is increased compared with control individuals ( $0.51 \pm 0.05$ ), suggesting a higher concentration of CT-longQ<sub>(disease)</sub> peptide fragments in the diseased state (Tsunemi et al., 2008; Tsou et al., 2011).

In our study, we found that long-term expression of CT-longQ27<sub>(disease)</sub> in cerebellar PCs leads to ataxia, associated with changes in PC firing and PC degeneration. These phenotypes are similar to phenotypes observed in other SCA6 knock-in mouse models, in which the length of the polyQ stretch had to be increased to 84 and 118 polyQs to cause disease symptoms (Watase et al., 2008; Unno et al., 2012). Compared with other mouse models, we now describe that CT-longQ27<sub>(disease)</sub>, but not CT-short, interferes with synaptic plasticity at the PF–PC synapse and causes the loss of EBC, an associative motor learning paradigm. The EBC is a withdrawal response to protect the eye from noxious stimuli and is mediated by a very defined cerebellar circuit with the requirement of functional PC plasticity (Kim and Thompson, 1997; De Zeeuw and Yeo, 2005; Gao et al., 2012). Indeed, loss of LTP at PF–PC synapses may be associated with changes in motor learning (Schonewille et al., 2010, 2011; Galliano et al., 2013). Conversely, LTD might also contribute (Kishimoto et al., 2001, 2002; Koekkoek et al., 2003), but this form of plasticity is probably less critical for EBC (Schonewille et al., 2011). Human subjects with cerebellar lesions and brain imaging studies also reveal an important role of the human cerebellum in EBC (Gerwig et al., 2007). Thus, the important aspect of this finding is that deficits in EBC in humans may also be associated with SCA6 as observed in our animal model and serve as a diagnostic clinical tool for early detection of SCA6 and other diseases associated with cerebellar dysfunction.

## Functional consequences of CT peptides expressed in PCs before cell death

Because CT-long is localized to the nucleus and the cytoplasm and has been identified as a transcription factor and a proteolytic product, changes in gene transcription and/or dominant-negative effects of the CT peptide might lead to functional alteration in PCs before cell death. In our experiments, the changes in synaptic plasticity and firing of PCs can be explained by

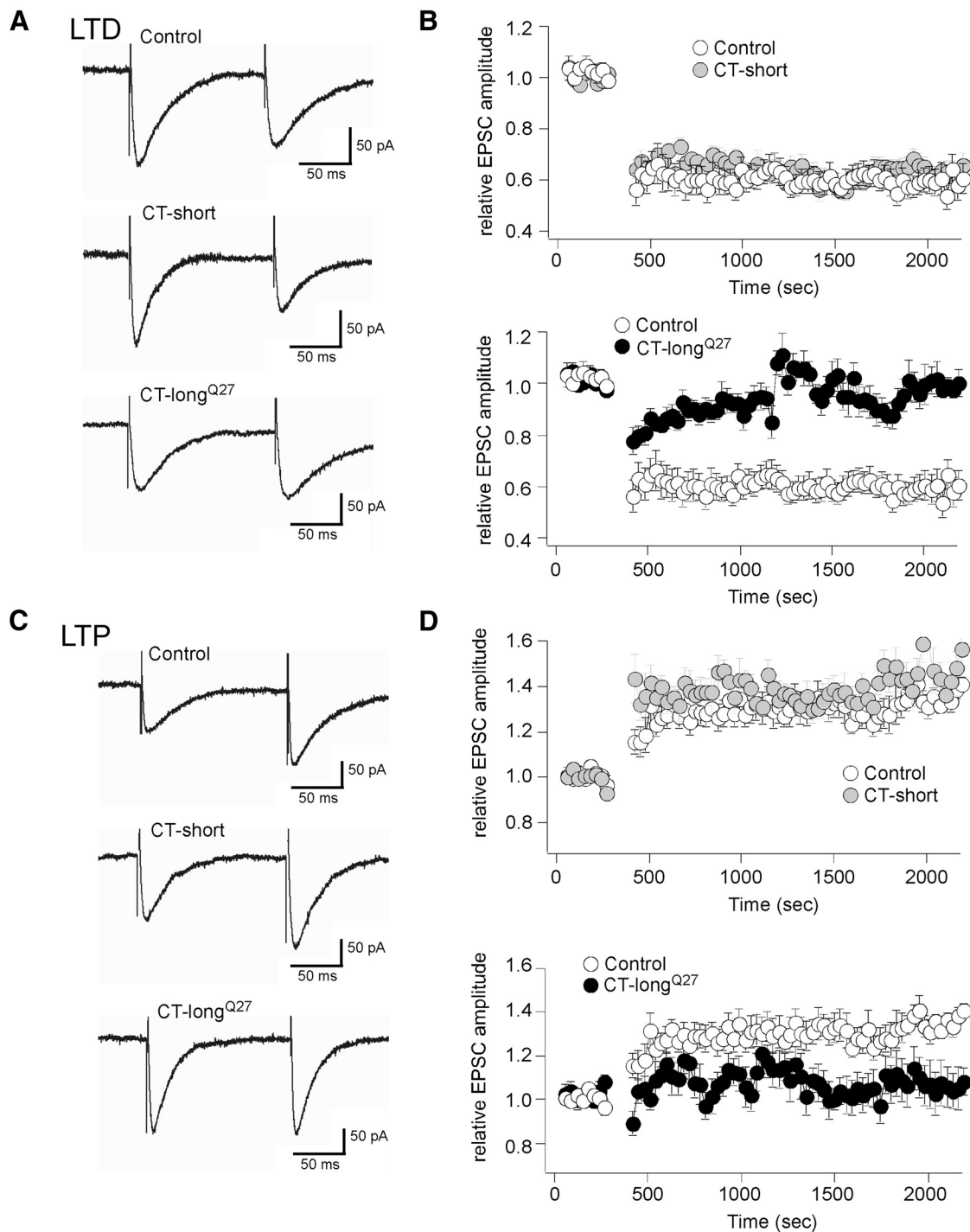


**Figure 8.** LTD and LTP at the PF–PC synapse of virally expressed CT-short and CT-longQ27 in the cerebellar cortex. **A, B**, LTD at the PF–PC synapse is blocked in the presence of CT-longQ27 but not CT-short. **A**, Representative PF-EPSC traces for control and CT-short- and CT-longQ27-expressing PCs before (left trace) and after (right trace) application of the LTD stimulation protocol. **B**, Time course of changes of PF-EPSC in PCs before and after application of the LTD stimulation protocol for CT-short-expressing (top) and CT-longQ27-expressing PCs. Conjunctive stimulation of PFs (1 Hz, 30 s) with depolarization to induce LTD was applied after 500 s. **C, D**, LTP at the PF–PC synapse was blocked in the presence of CT-longQ27 but not CT-short. **C**, Representative PF-EPSC traces for control and CT-short- and CT-longQ27-expressing PCs before (left trace) and after (right trace) application of the LTP stimulation protocol. **D**, Time course of changes of PF-EPSC in PCs before and after application of the LTP stimulation protocol for CT-short-expressing (top) and CT-longQ27-expressing (bottom) PCs. Conjunctive stimulation of PFs (1 Hz, 30 s) with depolarization to induce LTD was applied after 500 s.

dominant-negative effects of the CT domain on P/Q-type channel interacting proteins. The CT domain of the P/Q-type  $Ca^{2+}$  channel consists of binding domains for proteins involved in modulation, targeting, and structural organization of the channel complex in subcellular domains (Herlitze et al., 2003; Spafford et al., 2003). Therefore, a CT peptide expressed in the soma, axon,

or dendrites of PCs would be expected to induce dominant-negative effects on these parameters before PC degeneration. For example, P/Q-type channels are tightly coupled and colocalized to  $Ca^{2+}$ -activated  $K^+$  channels in PCs (Womack et al., 2004; Indriati et al., 2013). The functional interaction between these channels determines the mode and firing frequency of PCs.

Therefore, disruption of this interaction causes changes in the firing patterns of PCs similar to the alteration we observed with CT-longQ27. Indeed, chlorzoxazone, an activator of  $\text{Ca}^{2+}$ -activated  $\text{K}^+$  channels restores the precision of firing of PCs and improves motor behavior in both tottering and *Cacna1a*(S218L) mice, which are both ataxic P/Q-type channel mouse mutants (Alviña and Khodakhah, 2010). Furthermore, Berkefeld et al. (2006) demonstrated the formation of macromolecular complexes with  $\text{Ca}^{2+}$ -activated  $\text{K}^+$  channels and P/Q-type channels in rat brains. One can postulate that the CT peptide may be disrupting the formation of these  $\text{Ca}^{2+}$ -activated  $\text{K}^+$  channel–P/Q-type channel complexes by blocking critical binding sites on the  $\text{Ca}^{2+}$ -activated  $\text{K}^+$  channels or P/Q-type channels, thus leading to a disruption of these “ $\text{Ca}^{2+}$  nanodomains” necessary for  $\text{K}^+$  channel activation. In addition, the CT binds proteins involved in membrane transport and synapse assembly, such as the  $\text{Ca}_v\beta$  subunit (Herlitze et al., 2003). The multiple interaction sites within the CT domain of the P/Q-type  $\text{Ca}^{2+}$  channels make it a critical domain for the regulation of channel targeting to the membrane and synapses. Decreased clustering and current density of the channels have been demonstrated by the use of peptides that out-compete the interactions with Mint-1, CASK, and *tctex-1* (Spafford et al., 2003; Lai et al., 2005). The CT also contains binding sites for proteins involved in synaptic transmitter release, including Rim (Hibino et al., 2002; Shapira et al., 2003) and other proteins associated with Piccolo–Bassoon transport vesicles (Shapira et al., 2003). Because these proteins are involved in preforming synapses, CT peptides may interact with the clustering process required for synaptic targeting. Furthermore, the P/Q-type channel CT binds to proteins involved in synaptic plasticity, such as  $\text{Ca}^{2+}$ /calmodulin (Lee et al., 1999) and  $\text{Ca}^{2+}$  influx through dendritic P/Q-type channel, and is one of the major sources of dendritic  $\text{Ca}^{2+}$  necessary to induce LTD and LTP (Han et al., 2007). Therefore, changes in P/Q-type channel function in PCs in dendritic domains will most likely interfere with the expression of PC plasticity.

Dominant-negative effects on P/Q-type channel interacting proteins can be expected for both the CT-long and CT-short, because the described interacting proteins bind to both isoforms. However, we observed mainly behavioral and physiological effects for CT-longQ27 and not CT-short expressing PCs. The differences are most likely attributable to the different subcellular localization of the CTs within PCs. CT-short localizes mainly in the nucleus and at high expression levels diffuses throughout the cytoplasm. In contrast, CT-longQ27 is localized to cytoplasmic aggregates compatible with synaptic sites, in which it may compete with interacting proteins in subcellular domains.

In summary, we established a new SCA6 mouse model that will serve to understand the developmental onset of the disease and can be used for therapeutic drug testing. This mouse model develops late-onset ataxia associated with changes in PC firing and PC degeneration as observed in SCA6 patients. In addition, the mouse model identified the loss of EBC as a new diagnostic strategy for early detection of SCA6 in humans that is associated with changes in cerebellar plasticity.

## References

- Alviña K, Khodakhah K (2010) The therapeutic mode of action of 4-aminopyridine in cerebellar ataxia. *J Neurosci* 30:7258–7268. [CrossRef Medline](#)
- Barski JJ, Dethleffsen K, Meyer M (2000) Cre recombinase expression in cerebellar Purkinje cells. *Genesis* 28:93–98. [CrossRef Medline](#)
- Berkefeld H, Sailer CA, Bildl W, Rohde V, Thumfart JO, Eble S, Klugbauer N, Reisinger E, Bischofberger J, Oliver D, Knaus HG, Schulte U, Fakler B

- (2006) BKCa-Cav channel complexes mediate rapid and localized  $\text{Ca}^{2+}$ -activated  $\text{K}^+$  signaling. *Science* 314:615–620. [CrossRef Medline](#)
- Bidaud I, Mezghrani A, Wayne LA, Monteil A, Lory P (2006) Voltage-gated calcium channels in genetic diseases. *Biochim Biophys Acta* 1763:1169–1174. [CrossRef Medline](#)
- Boele HJ, Koekoek SK, De Zeeuw CI (2010) Cerebellar and extracerebellar involvement in mouse eyeblink conditioning: the ACDC model. *Front Cell Neurosci* 3:19. [CrossRef Medline](#)
- Boele HJ, Koekoek SK, De Zeeuw CI, Ruigrok TJ (2013) Axonal sprouting and formation of terminals in the adult cerebellum during associative motor learning. *J Neurosci* 33:17897–17907. [CrossRef Medline](#)
- Braz JM, Rico B, Basbaum AI (2002) Transneuronal tracing of diverse CNS circuits by Cre-mediated induction of wheat germ agglutinin in transgenic mice. *Proc Natl Acad Sci U S A* 99:15148–15153. [CrossRef Medline](#)
- De Zeeuw CI, Yeo CH (2005) Time and tide in cerebellar memory formation. *Curr Opin Neurobiol* 15:667–674. [CrossRef Medline](#)
- De Zeeuw CI, Hoebeek FE, Bosman LW, Schonewille M, Witter L, Koekoek SK (2011) Spatiotemporal firing patterns in the cerebellum. *Nat Rev Neurosci* 12:327–344. [CrossRef Medline](#)
- Du X, Wang J, Zhu H, Rinaldo L, Lamar KM, Palmenberg AC, Hansel C, Gomez CM (2013) Second cistron in *CACNA1A* gene encodes a transcription factor mediating cerebellar development and SCA6. *Cell* 154:118–133. [CrossRef Medline](#)
- Galliano E, Gao Z, Schonewille M, Todorov B, Simons E, Pop AS, D’Angelo E, van den Maagdenberg AM, Hoebeek FE, De Zeeuw CI (2013) Silencing the majority of cerebellar granule cells uncovers their essential role in motor learning and consolidation. *Cell Rep* 3:1239–1251. [CrossRef Medline](#)
- Gao Z, van Beugen BJ, De Zeeuw CI (2012) Distributed synergistic plasticity and cerebellar learning. *Nat Rev Neurosci* 13:619–635. [CrossRef Medline](#)
- Gerwig M, Kolb FP, Timmann D (2007) The involvement of the human cerebellum in eyeblink conditioning. *Cerebellum* 6:38–57. [CrossRef Medline](#)
- Han J, Mark MD, Li X, Xie M, Waka S, Rettig J, Herlitze S (2006) RGS2 determines short-term synaptic plasticity in hippocampal neurons by regulating Gi/o-mediated inhibition of presynaptic  $\text{Ca}^{2+}$  channels. *Neuron* 51:575–586. [CrossRef Medline](#)
- Han VZ, Zhang Y, Bell CC, Hansel C (2007) Synaptic plasticity and calcium signaling in Purkinje cells of the central cerebellar lobes of mormyrid fish. *J Neurosci* 27:13499–13512. [CrossRef Medline](#)
- Herlitze S, Xie M, Han J, Hümmer A, Melnik-Martinez KV, Moreno RL, Mark MD (2003) Targeting mechanisms of high voltage-activated  $\text{Ca}^{2+}$  channels. *J Bioenerg Biomembr* 35:621–637. [CrossRef Medline](#)
- Hibino H, Pironkova R, Onwumere O, Vologodskaya M, Hudspeth AJ, Lesage F (2002) RIM binding proteins (RBPs) couple Rab3-interacting molecules (RIMs) to voltage-gated  $\text{Ca}^{2+}$  channels. *Neuron* 34:411–423. [CrossRef Medline](#)
- Indriati DW, Kamasawa N, Matsui K, Meredith AL, Watanabe M, Shigemoto R (2013) Quantitative localization of *cav2.1* (p/q-type) voltage-dependent calcium channels in purkinje cells: somatodendritic gradient and distinct somatic coclustering with calcium-activated potassium channels. *J Neurosci* 33:3668–3678. [CrossRef Medline](#)
- Ishiguro T, Ishikawa K, Takahashi M, Obayashi M, Amino T, Sato N, Sakamoto M, Fujigasaki H, Tsuruta F, Dolmetsch R, Arai T, Sasaki H, Nagashima K, Kato T, Yamada M, Takahashi H, Hashizume Y, Mizusawa H (2010) The carboxy-terminal fragment of  $\alpha$ (1A) calcium channel preferentially aggregates in the cytoplasm of human spinocerebellar ataxia type 6 Purkinje cells. *Acta Neuropathol* 119:447–464. [CrossRef Medline](#)
- Ishikawa K, Fujigasaki H, Saegusa H, Ohwada K, Fujita T, Iwamoto H, Komatsuzaki Y, Toru S, Toriyama H, Watanabe M, Ohkoshi N, Shoji S, Kanazawa I, Tanabe T, Mizusawa H (1999a) Abundant expression and cytoplasmic aggregations of  $\alpha$ (1A) voltage-dependent calcium channel protein associated with neurodegeneration in spinocerebellar ataxia type 6. *Hum Mol Genet* 8:1185–1193. [CrossRef Medline](#)
- Ishikawa K, Watanabe M, Yoshizawa K, Fujita T, Iwamoto H, Yoshizawa T, Harada K, Nakamagoe K, Komatsuzaki Y, Satoh A, Doi M, Ogata T, Kanazawa I, Shoji S, Mizusawa H (1999b) Clinical, neuropathological, and molecular study in two families with spinocerebellar ataxia type 6 (SCA6). *J Neurol Neurosurg Psychiatry* 67:86–89. [CrossRef Medline](#)
- Ishikawa K, Owada K, Ishida K, Fujigasaki H, Shun Li M, Tsunemi T, Ohkoshi N, Toru S, Mizutani T, Hayashi M, Arai N, Hasegawa K, Kawanami T, Kato T, Makifuchi T, Shoji S, Tanabe T, Mizusawa H (2001) Cytoplasmic and nuclear polyglutamine aggregates in SCA6 Purkinje cells. *Neurology* 56:1753–1756. [CrossRef Medline](#)

- Kim JJ, Thompson RF (1997) Cerebellar circuits and synaptic mechanisms involved in classical eyeblink conditioning. *Trends Neurosci* 20:177–181. [CrossRef Medline](#)
- Kishimoto Y, Kawahara S, Fujimichi R, Mori H, Mishina M, Kirino Y (2001) Impairment of eyeblink conditioning in GluRdelta2-mutant mice depends on the temporal overlap between conditioned and unconditioned stimuli. *Eur J Neurosci* 14:1515–1521. [CrossRef Medline](#)
- Kishimoto Y, Fujimichi R, Araishi K, Kawahara S, Kano M, Aiba A, Kirino Y (2002) mGluR1 in cerebellar Purkinje cells is required for normal association of temporally contiguous stimuli in classical conditioning. *Eur J Neurosci* 16:2416–2424. [CrossRef Medline](#)
- Koekkoek SK, Den Ouden WL, Perry G, Highstein SM, De Zeeuw CI (2002) Monitoring kinetic and frequency-domain properties of eyelid responses in mice with magnetic distance measurement technique. *J Neurophysiol* 88:2124–2133. [Medline](#)
- Koekkoek SK, Hulscher HC, Dortland BR, Hensbroek RA, Elgersma Y, Ruigrok TJ, De Zeeuw CI (2003) Cerebellar LTD and learning-dependent timing of conditioned eyelid responses. *Science* 301:1736–1739. [CrossRef Medline](#)
- Koeppen AH (2005) The pathogenesis of spinocerebellar ataxia. *Cerebellum* 4:62–73. [CrossRef Medline](#)
- Kordasiewicz HB, Thompson RM, Clark HB, Gomez CM (2006) C-termini of P/Q-type Ca<sup>2+</sup> channel alpha1A subunits translocate to nuclei and promote polyglutamine-mediated toxicity. *Hum Mol Genet* 15:1587–1599. [CrossRef Medline](#)
- Kruse W, Krause M, Aarse J, Mark MD, Manahan-Vaughan D, Herlitze S (2014) Optogenetic modulation and multi-electrode analysis of cerebellar networks in vivo. *PLoS One* 9:e105589. [CrossRef Medline](#)
- Kubodera T, Yokota T, Ohwada K, Ishikawa K, Miura H, Matsuoka T, Mizusawa H (2003) Proteolytic cleavage and cellular toxicity of the human alpha1A calcium channel in spinocerebellar ataxia type 6. *Neurosci Lett* 341:74–78. [CrossRef Medline](#)
- Lai M, Wang F, Rohan JG, Maeno-Hikichi Y, Chen Y, Zhou Y, Gao G, Sather WA, Zhang JF (2005) A tctex1-Ca<sup>2+</sup> channel complex for selective surface expression of Ca<sup>2+</sup> channels in neurons. *Nat Neurosci* 8:435–442. [CrossRef Medline](#)
- Lee A, Wong ST, Gallagher D, Li B, Storm DR, Scheuer T, Catterall WA (1999) Ca<sup>2+</sup>/calmodulin binds to and modulates P/Q-type calcium channels. *Nature* 399:155–159. [CrossRef Medline](#)
- Maejima T, Wollenweber P, Teusner LU, Noebels JL, Herlitze S, Mark MD (2013) Postnatal loss of P/Q-type channels confined to rhombic-lip-derived neurons alters synaptic transmission at the parallel fiber to Purkinje cell synapse and replicates genomic cacna1a mutation phenotype of ataxia and seizures in mice. *J Neurosci* 33:5162–5174. [CrossRef Medline](#)
- Mantuano E, Veneziano L, Jodice C, Frontali M (2003) Spinocerebellar ataxia type 6 and episodic ataxia type 2: differences and similarities between two allelic disorders. *Cytogenet Genome Res* 100:147–153. [CrossRef Medline](#)
- Mark MD, Maejima T, Kuckelsberg D, Yoo JW, Hyde RA, Shah V, Gutierrez D, Moreno RL, Kruse W, Noebels JL, Herlitze S (2011) Delayed postnatal loss of P/Q-type calcium channels recapitulates the absence epilepsy, dyskinesia, and ataxia phenotypes of genomic Cacna1A mutations. *J Neurosci* 31:4311–4326. [CrossRef Medline](#)
- Orr HT (2012) Cell biology of spinocerebellar ataxia. *J Cell Biol* 197:167–177. [CrossRef Medline](#)
- Pietrobon D (2005) Function and dysfunction of synaptic calcium channels: insights from mouse models. *Curr Opin Neurobiol* 15:257–265. [CrossRef Medline](#)
- Pietrobon D (2010) CaV2.1 channelopathies. *Pflugers Arch* 460:375–393. [CrossRef Medline](#)
- Quinn LP, Perren MJ, Brackenborough KT, Woodhams PL, Vidgeon-Hart M, Chapman H, Pangalos MN, Upton N, Virley DJ (2007) A beam-walking apparatus to assess behavioural impairments in MPTP-treated mice: pharmacological validation with R-(−)-deprenyl. *J Neurosci Methods* 164:43–49. [CrossRef Medline](#)
- Saegusa H, Wakamori M, Matsuda Y, Wang J, Mori Y, Zong S, Tanabe T (2007) Properties of human Cav2.1 channel with a spinocerebellar ataxia type 6 mutation expressed in Purkinje cells. *Mol Cell Neurosci* 34:261–270. [CrossRef Medline](#)
- Schmoleky MT, Weber JT, De Zeeuw CI, Hansel C (2002) The making of a complex spike: ionic composition and plasticity. *Ann N Y Acad Sci* 978:359–390. [CrossRef Medline](#)
- Schonewille M, Khosrovani S, Winkelman BH, Hoebeek FE, De Jeu MT, Larsen IM, Van der Burg J, Schmoleky MT, Frens MA, De Zeeuw CI (2006) Purkinje cells in awake behaving animals operate at the upstate membrane potential. *Nat Neurosci* 9:459–461. [CrossRef Medline](#)
- Schonewille M, Belmeguenai A, Koekkoek SK, Houtman SH, Boele HJ, van Beugen BJ, Gao Z, Badura A, Ohtsuki G, Amerika WE, Hossy E, Hoebeek FE, Elgersma Y, Hansel C, De Zeeuw CI (2010) Purkinje cell-specific knockout of the protein phosphatase PP2B impairs potentiation and cerebellar motor learning. *Neuron* 67:618–628. [CrossRef Medline](#)
- Schonewille M, Gao Z, Boele HJ, Veloz MF, Amerika WE, Simek AA, De Jeu MT, Steinberg JP, Takamiya K, Hoebeek FE, Linden DJ, Huganir RL, De Zeeuw CI (2011) Reevaluating the role of LTD in cerebellar motor learning. *Neuron* 70:43–50. [CrossRef Medline](#)
- Shapira M, Zhai RG, Dresbach T, Bresler T, Torres VI, Gundelfinger ED, Ziv NE, Garner CC (2003) Unitary assembly of presynaptic active zones from Piccolo-Bassoon transport vesicles. *Neuron* 38:237–252. [CrossRef Medline](#)
- Soong TW, DeMaria CD, Alvania RS, Zweifel LS, Liang MC, Mittman S, Agnew WS, Yue DT (2002) Systematic identification of splice variants in human P/Q-type channel alpha1(2.1) subunits: implications for current density and Ca<sup>2+</sup>-dependent inactivation. *J Neurosci* 22:10142–10152. [Medline](#)
- Spafford JD, Munno DW, Van Nierop P, Feng ZP, Jarvis SE, Gallin WJ, Smit AB, Zamponi GW, Syed NI (2003) Calcium channel structural determinants of synaptic transmission between identified invertebrate neurons. *J Biol Chem* 278:4258–4267. [CrossRef Medline](#)
- Spoida K, Massek OA, Deneris ES, Herlitze S (2014) Gq/5-HT2c receptor signals activate a local GABAergic inhibitory feedback circuit to modulate serotonergic firing and anxiety in mice. *Proc Natl Acad Sci U S A* 111:6479–6484. [CrossRef Medline](#)
- Takahashi M, Obayashi M, Ishiguro T, Sato N, Niimi Y, Ozaki K, Mogushi K, Mahmut Y, Tanaka H, Tsuruta F, Dolmetsch R, Yamada M, Takahashi H, Kato T, Mori O, Eishi Y, Mizusawa H, Ishikawa K (2013) Cytoplasmic location of alpha1A voltage-gated calcium channel C-terminal fragment (Cav2.1-CTF) aggregate is sufficient to cause cell death. *PLoS One* 8:e50121. [CrossRef Medline](#)
- Tsou WL, Soong BW, Paulson HL, Rodríguez-Lebrón E (2011) Splice isoform-specific suppression of the Cav2.1 variant underlying spinocerebellar ataxia type 6. *Neurobiol Dis* 43:533–542. [CrossRef Medline](#)
- Tsunemi T, Ishikawa K, Jin H, Mizusawa H (2008) Cell-type-specific alternative splicing in spinocerebellar ataxia type 6. *Neurosci Lett* 447:78–81. [CrossRef Medline](#)
- Unno T, Wakamori M, Koike M, Uchiyama Y, Ishikawa K, Kubota H, Yoshida T, Sasaki H, Peters C, Mizusawa H, Watake K (2012) Development of Purkinje cell degeneration in a knockin mouse model reveals lysosomal involvement in the pathogenesis of SCA6. *Proc Natl Acad Sci U S A* 109:17693–17698. [CrossRef Medline](#)
- Watake K, Barrett CF, Miyazaki T, Ishiguro T, Ishikawa K, Hu Y, Unno T, Sun Y, Kasai S, Watanabe M, Gomez CM, Mizusawa H, Tsien RW, Zoghbi HY (2008) Spinocerebellar ataxia type 6 knockin mice develop a progressive neuronal dysfunction with age-dependent accumulation of mutant Cav2.1 channels. *Proc Natl Acad Sci U S A* 105:11987–11992. [CrossRef Medline](#)
- Womack M, Khodakhah K (2002) Active contribution of dendrites to the tonic and trimodal patterns of activity in cerebellar Purkinje neurons. *J Neurosci* 22:10603–10612. [Medline](#)
- Womack MD, Khodakhah K (2003) Somatic and dendritic small-conductance calcium-activated potassium channels regulate the output of cerebellar Purkinje neurons. *J Neurosci* 23:2600–2607. [Medline](#)
- Womack MD, Chevez C, Khodakhah K (2004) Calcium-activated potassium channels are selectively coupled to P/Q-type calcium channels in cerebellar Purkinje neurons. *J Neurosci* 24:8818–8822. [CrossRef Medline](#)
- Xu X, Scott MM, Deneris ES (2006) Shared long-range regulatory elements coordinate expression of a gene cluster encoding nicotinic receptor heteromeric subtypes. *Mol Cell Biol* 26:5636–5649. [CrossRef Medline](#)
- Yartsev MM, Givon-Mayo R, Maller M, Donchin O (2009) Pausing purkinje cells in the cerebellum of the awake cat. *Front Syst Neurosci* 3:2. [CrossRef Medline](#)
- Zhuchenko O, Bailey J, Bonnen P, Ashizawa T, Stockton DW, Amos C, Dobyns WB, Subramony SH, Zoghbi HY, Lee CC (1997) Autosomal dominant cerebellar ataxia (SCA6) associated with small polyglutamine expansions in the alpha 1A-voltage-dependent calcium channel. *Nat Genet* 15:62–69. [CrossRef Medline](#)
- Zoghbi HY, Orr HT (2000) Glutamine repeats and neurodegeneration. *Annu Rev Neurosci* 23:217–247. [CrossRef Medline](#)